ALTERNATIVE APPROACHES FOR UTILIZING LIDAR DATA AS A SOURCE OF CONTROL INFORMATION FOR PHOTOGRAMMETRIC MODELS

A. F. Habib [a], M. S. Ghanma [a], C. J. Kim [a], E. Mitishita [b]

[a] Department of Geomatics Engineering, University of Calgary
2500, University Drive NW, Calgary AB T2N 1N4 Canada – (habib, mghanma)@geomatics.ucalgary.ca, Cjkim@ucalgary.ca,
[b] Departamento de Geomática, Universidade Federal Do Paraná, Caixa Postal 19.001, 81.531-970 Curitiba, Paraná, Brasil
mitishita@ufpr.br

WG I/5 Platform and Sensor Integration

KEY WORDS: Laser Scanning, LIDAR Intensity, Photogrammetry, Linear Features, Absolute Orientation.

ABSTRACT:

Laser scanning (LIDAR) is a recent technology that is receiving an increasing interest from professionals dealing with mapping applications. The interest in LIDAR is attributed to the rich geometric surface information provided by the data in the form of dense non-selective points. On the other hand, photogrammetric processing of stereo-images provides an accurate surface model represented by few points as well as a wealth of semantic information about the photographed objects. Considering the nature of photogrammetric and LIDAR data, it is clear that the two systems provide complementary information. However, the complementary information can only be fully utilized after successful alignment/absolute orientation of the photogrammetric and LIDAR models relative to a common reference frame. This paper deals with two alternative approaches for utilizing linear features derived from LIDAR data as control information for aligning the photogrammetric model relative to the LIDAR reference frame. The first approach incorporates LIDAR lines as control information directly in a photogrammetric triangulation. The second approach starts by generating a photogrammetric model through a photogrammetric triangulation using an arbitrary datum (no control information). LIDAR features are then used as control information for the absolute orientation of the photogrammetric model. A mathematical model is derived to utilize the LIDAR features for the absolute orientation of the photogrammetric model. These features can be extracted from range data using various methods. For example, planar patches can be extracted from 3-dimensional LIDAR data through segmentation techniques. Then, neighbouring planar patches can be intersected to generate linear features corresponding to object space discontinuities. LIDAR data pre-processing for the purpose of feature extraction is not a trivial task. An alternative and simpler approach is to use recorded intensities by laser scanners to directly identify and extract linear features from the LIDAR data. The paper presents a quantitative analysis of the performance of the different approaches for extracting linear features from the LIDAR data. The analysis is based on the quality of fit of the final alignment between the LIDAR and photogrammetric models.

1. INTRODUCTION

Light Detection and Ranging (LIDAR) is a modern technology, which has received wide acceptance and popularity due to its usefulness in mapping applications. Since the introduction of LIDAR in the mapping industry, its applications in GIS and other areas have multiplied. On the other side, photogrammetry is a well established mapping and surface reconstruction technique. However, the continuous development of LIDAR systems in the aspects of reduced hardware size and increased resolution and density, made it an increasingly favoured option in a variety of applications especially where rapid and accurate data collection on physical surface is required (Schenk and Csathó, 2002).

Photogrammetric data is characterized by high redundancy through observing desired features in multiple images, making it more suited for mapping heavily populated areas. Richness in semantic information and dense positional data along object space break lines add to its advantages. Nonetheless, photogrammetry has its own drawbacks; where there is almost no positional information along homogeneous surfaces and vertical accuracy is worse than the planimetric accuracy. A major obstacle in the way of automation in photogrammetry is the complicated and sometimes unreliable matching procedure especially when dealing with large scale imagery over urban areas.

LIDAR, on the other hand, is a direct acquisition of positional information. Also it produces dense information along homogeneous surfaces, making it preferable in mapping Polar Regions. Still, LIDAR possesses few undesirable features that make it incapable of being a standalone reliable technology. LIDAR data has no redundancy and almost has no positional information along object space break-lines. Also, the planimetric accuracy is worse than the vertical, in addition to LIDAR data lacking semantic information.

Both, photogrammetry and LIDAR, have unique characteristics that make them preferable in specific applications. One can observe that a negative aspect in one technology is contrasted by an opposite strength in the other. Hence, integrating the two systems would prove beneficial resulting in more understanding of information associated with physical surfaces (Baltsavias, 1999). However, the complementary information can only be fully utilized after successful alignment/absolute orientation of the photogrammetric and LIDAR models relative to a common reference frame. (Postolov et al., 1999).

The majority of registration methodologies rely on point primitives for solving the registration problem between two datasets. Such methodologies are not applicable to LIDAR

surfaces since they correspond to laser footprints instead of distinct points that could be identified in imagery (Baltsavias, 1999). Conventionally, surface-to-surface registration and comparison have been achieved by interpolating both datasets into a uniform grid. The comparison is then reduced to estimating the necessary shifts by analyzing the elevations at corresponding grid posts (Ebner and Ohlhof, 1994; Kilian et al., 1996). Several issues can arise with this approach. First, the interpolation to a grid will introduce errors especially when dealing with captured surfaces over urban areas. Moreover, minimizing the differences between surfaces along the z-direction is only valid when dealing with horizontal planar surfaces (Habib and Schenk, 1999). Postolov et al. (1999) presented another approach, which works on the original scattered data without prior interpolation. However, the implementation procedure involves an interpolation of one surface at the location of conjugate points on the other surface. Additionally, the registration is based on minimizing the differences between the two surfaces along the z-direction. Schenk (1999) introduced an alternative approach, where distances between points of one surface along surface normals to locally interpolated patches of the other surface are minimized. Habib et al. (2001) implemented this methodology within a comprehensive automatic registration procedure. Such an approach is based on processing the photogrammetric data to produce object space planar patches. This might not be always possible since photogrammetric surfaces provide accurate information along object space discontinuities while supplying almost no information along homogeneous surfaces with uniform texture.

This paper deals with alternative approaches for utilizing linear features derived from LIDAR data as control information for aligning the photogrammetric model relative to the LIDAR reference frame. The following section addresses the general methodology and mathematical models of the suggested approaches including the techniques adopted for extracting the registration primitives from photogrammetric and LIDAR data. The last two sections cover experimental results (using aerial datasets) as well as conclusions and recommendations for future work.

2. METHODOLOGY

In this paper, two approaches will be applied to incorporate LIDAR lines in aligning the photogrammetric model to the LIDAR reference frame. The first approach incorporates LIDAR lines as control information directly in a photogrammetric triangulation. The second approach starts by generating a photogrammetric model through a photogrammetric triangulation using an arbitrary datum (no control information). LIDAR features are then used as control for the absolute orientation of the photogrammetric model.

2.1 Approach 1: Direct involvement of LIDAR lines in photogrammetric triangulation

Conjugate linear features in the photogrammetric and LIDAR datasets should first be extracted and then incorporated in a photogrammetric triangulation in which LIDAR lines will act as the source of control to align the photogrammetric model. The following subsections describe the procedures adopted to extract straight line features in both datasets and how they are included in the overall alignment procedure.

Photogrammetric straight-line features

The methodology for producing 3-D straight line features from photogrammetric datasets depends on the representation scheme of such features in the object and image space. Prior research in this area concluded that representing object space straight lines using two points along the line is the most convenient representation from a photogrammetric point of view since it yields well-defined line segments (Habib et al., 2002). On the other hand, image space lines will be represented by a sequence of 2-D coordinates of intermediate points along the feature. This representation is attractive since it can handle image space linear features in the presence of distortions as they will cause deviations from straightness.

In general, the manipulation of tie straight lines appearing in a group of overlapping images starts by identifying two points in one (Figure 1a) or two images (Figure 1b) along the line under consideration. These points will be used to define the corresponding object space line segment. One should note that these points need not be identifiable or even visible in other images. Intermediate points along the line are measured in all the overlapping images. Similar to the end points, the intermediate points need not be conjugate, Figure 1.

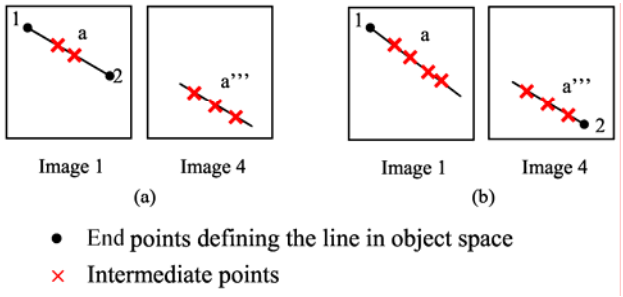

Figure 1: End points defining the object line are either measured in one image (a) or two images (b).

For the end points, the relationship between the measured image coordinates $\{(x_1, y_1), (x_2, y_2)\}$ and the corresponding ground coordinates $\{(X_1, Y_1, Z_1), (X_2, Y_2, Z_2)\}$ is established through the collinearity equations. Only four equations will be written for each line. The incorporation of intermediate points into the adjustment procedure is achieved through a mathematical constraint. The underlying principle in this constraint is that the vector from the perspective centre to any intermediate image point along the line is contained within the plane defined by the perspective centre of that image and the two points defining the straight line in the object space, Figure 2. This can be mathematically described through Equation 1.

$$\left(\vec{V}_1 \times \vec{V}_2\right) \bullet \vec{V}_3 = 0 \qquad (1)$$

In the above equation, $\vec{V}_1$ is the vector connecting the perspective centre to the first end point along the object space line, $\vec{V}_2$ is the vector connecting the perspective centre to the second end point along the object space line, and $\vec{V}_3$ is the vector connecting the perspective centre to an intermediate point along the corresponding image line. It should be noted that the three vectors should be represented relative to a common coordinate system (e.g., the ground coordinate system). The constraint in Equation 1 incorporates the image coordinates of the intermediate point, the Exterior Orientation Parameters (EOP), the Interior Orientation Parameters (IOP)

including distortion parameters, as well as the ground coordinates of the points defining the object space line. Such a constraint does not introduce any new parameters and can be written for all intermediate points along the line in the imagery. The number of constraints is equal to the number of intermediate points measured along the image line.

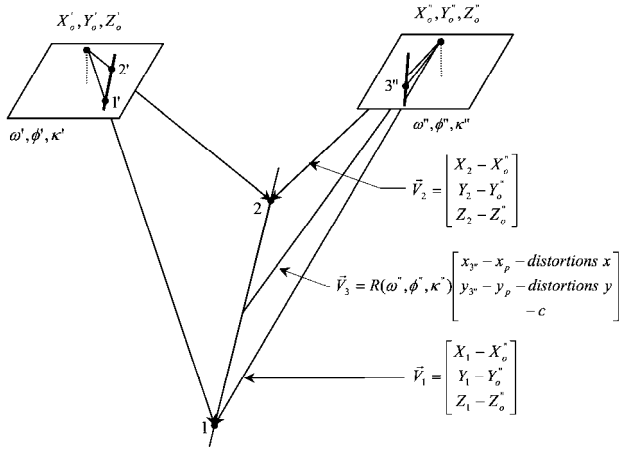

Figure 2: Perspective transformation between image and object space straight lines.

As a special case of the above procedure, the treatment of control linear features (with known object coordinates of its end points) will be slightly different. The control line will provide the end points in the object space; hence, these end points need not be measured in any of the images and no collinearity equations will be written for any of the control lines. Subsequently, image space linear features are represented only by a group of intermediate points measured in all images.

LIDAR straight-line features

The growing acceptance of LIDAR as an efficient data acquisition system by researchers in the photogrammetric community led to a number of studies aiming at pre-processing LIDAR data. The purpose of such studies ranges from simple primitive detection and extraction to more complicated tasks such as segmentation and perceptual organization (Maas and Vosselman, 1999; Csathó et al., 1999; Lee and Schenk, 2001; Filin, 2002).

In this paper, LIDAR straight line features will be used as a source of control for photogrammetric models. To extract such lines, suspected planar patches in a LIDAR dataset are manually identified with the help of corresponding optical imagery, Figure 3. The selected patches are then checked using a least squares adjustment to determine whether they are planar or not and to remove blunders. Finally, neighbouring planar patches with different orientation are intersected to determine the end points along object space discontinuities between the patches under consideration.

In another approach to simplify the extraction process, intensity and range data recorded by the LIDAR system are utilized for direct measurement of linear features. Raw range and intensity data are first interpolated to a uniform grid using identical interpolation method and parameters. Linear features previously extracted from photogrammetry are then identified on the intensity image from which planimetric coordinates of line ends are measured while observing height readings from the range image, Figure 4. It is worth mentioning that the interpolation method and applied parameters have a visible effect on the accuracy of this approach.

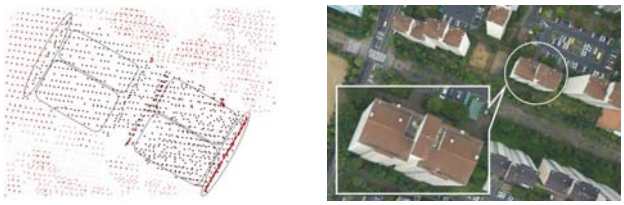

(a) (b)

Figure 3: Manually identified planar patches within the LIDAR data (a) guided by the corresponding optical image (b).

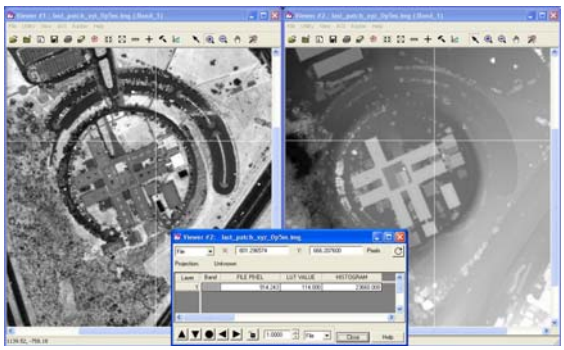

(a) (b)

Figure 4: Manually measuring planimetric coordinates from intensity image (a) and height from range image (b).

2.2 Approach 2: Using LIDAR lines in the absolute orientation of photogrammetric model

This approach starts with generating a photogrammetric model through a photogrammetric triangulation using an arbitrary datum without knowledge of any control information. The datum is achieved through fixing 7 coordinates of three well-distributed points in the bundle adjustment procedure. The next step is determining the elements of the absolute orientation parameters to align this photogrammetric model to the LIDAR reference frame using conjugate straight line segments. Both photogrammetric and LIDAR line segments are represented by their end points. These end points are not required to be conjugate. In this paper, a 3D similarity transformation is used, Equation 2.

$$\begin{bmatrix} X_A \\ Y_A \\ Z_A \end{bmatrix} = \begin{bmatrix} X_T \\ Y_T \\ Z_T \end{bmatrix} + S\ R(\omega, \phi, \kappa) \begin{bmatrix} X_a \\ Y_a \\ Z_a \end{bmatrix} \qquad (2)$$

Where S is the scale factor, $(X_T\ Y_T\ Z_T)^T$ is the translation vector between the origins of the photogrammetric and LIDAR coordinate systems, R is the 3D orthogonal rotation matrix, $(X_a\ Y_a\ Z_a)^T$ are the point coordinates in one dataset, while $(X_A\ Y_A\ Z_A)^T$ are the point coordinates in the other.

Referring to Figure 5, the two points describing the line segment from the photogrammetric model undergo a 3-D similarity transformation onto the line segment AB from the LIDAR dataset. The objective here is to introduce the necessary constraints to describe the fact that the model segment (12)

coincides with the object segment (AB) after applying the absolute orientation.

For the photogrammetric point (1), this constraint can be mathematically described by Equation 3.

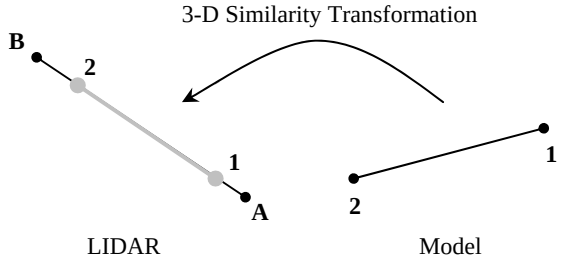

Figure 5: Similarity measure between photogrammetric and LIDAR linear features.

$$\begin{bmatrix} X_T \\ Y_T \\ Z_T \end{bmatrix} + S\ R_{(\Omega,\Phi,K)} \begin{bmatrix} X_1 \\ Y_1 \\ Z_1 \end{bmatrix} = \begin{bmatrix} X_A \\ Y_A \\ Z_A \end{bmatrix} + \lambda_1 \begin{bmatrix} X_B - X_A \\ Y_B - Y_A \\ Z_B - Z_A \end{bmatrix} \quad (3)$$

Equation 4 shows the constraint for point (2).

$$\begin{bmatrix} X_T \\ Y_T \\ Z_T \end{bmatrix} + S\ R_{(\Omega,\Phi,K)} \begin{bmatrix} X_2 \\ Y_2 \\ Z_2 \end{bmatrix} = \begin{bmatrix} X_A \\ Y_A \\ Z_A \end{bmatrix} + \lambda_2 \begin{bmatrix} X_B - X_A \\ Y_B - Y_A \\ Z_B - Z_A \end{bmatrix} \quad (4)$$

where λ_1 and λ_2 are scale factors.

Subtracting Equation 4 from Equation 3 yields:

$$(\lambda_2 - \lambda_1) \begin{bmatrix} X_B - X_A \\ Y_B - Y_A \\ Z_B - Z_A \end{bmatrix} = S\ R_{(\Omega,\Phi,K)} \begin{bmatrix} X_2 - X_1 \\ Y_2 - Y_1 \\ Z_2 - Z_1 \end{bmatrix} \quad (5)$$

Equation 5 emphasizes the concept that model line segments should be parallel to the object line segments after applying the rotation matrix. To recover the elements of the rotation matrix, Equation 5 is further manipulated and rearranged starting by dividing the first and second rows by the third to eliminate the scale factors, Equations 6.

$$\frac{(X_B - X_A)}{(Z_B - Z_A)} = \frac{R_{11}(X_2 - X_1) + R_{12}(Y_2 - Y_1) + R_{13}(Z_2 - Z_1)}{R_{31}(X_2 - X_1) + R_{32}(Y_2 - Y_1) + R_{33}(Z_2 - Z_1)}$$
$$\frac{(Y_B - Y_A)}{(Z_B - Z_A)} = \frac{R_{21}(X_2 - X_1) + R_{22}(Y_2 - Y_1) + R_{23}(Z_2 - Z_1)}{R_{31}(X_2 - X_1) + R_{32}(Y_2 - Y_1) + R_{33}(Z_2 - Z_1)} \quad (6)$$

A pair of conjugate line segments yields two equations, which contribute towards the estimation of two rotation angles, the azimuth and pitch angle along the line. On the other hand, the roll angle across the line cannot be estimated. Hence a minimum of two non-parallel lines is needed to recover the three elements of the rotation matrix (Ω,Φ,K).

Now, the scale factor and the shift components are to be determined. Starting by applying the rotation matrix to the coordinates of the first point defining the photogrammetric line, Equation 7 is written.

$$\begin{bmatrix} X_T \\ Y_T \\ Z_T \end{bmatrix} + S \begin{bmatrix} x_1 \\ y_1 \\ z_1 \end{bmatrix} = \begin{bmatrix} X_A \\ Y_A \\ Z_A \end{bmatrix} + \lambda_1 \begin{bmatrix} X_B - X_A \\ Y_B - Y_A \\ Z_B - Z_A \end{bmatrix} \quad (7)$$

where,

$$\begin{bmatrix} x_1 & y_1 & z_1 \end{bmatrix}^T = R_{(\Omega,\Phi,K)} \begin{bmatrix} X_1 & Y_1 & Z_1 \end{bmatrix}^T$$

Rearranging the terms yields:

$$\lambda_1 \begin{bmatrix} X_B - X_A \\ Y_B - Y_A \\ Z_B - Z_A \end{bmatrix} = \begin{bmatrix} X_T + S\,x_1 - X_A \\ Y_T + S\,y_1 - Y_A \\ Z_T + S\,z_1 - Z_A \end{bmatrix} \quad (8)$$

In Equation 8, λ_1 is eliminated by dividing the first and second rows by the third, Equations 9. The same applies to point 2 and Equations 10 can be written.

$$\frac{(X_B - X_A)}{(Z_B - Z_A)} = \frac{(X_T + S\,x_1 - X_A)}{(Z_T + S\,z_1 - Z_A)},\quad \frac{(Y_B - Y_A)}{(Z_B - Z_A)} = \frac{(Y_T + S\,y_1 - Y_A)}{(Z_T + S\,z_1 - Z_A)} \quad (9)$$

$$\frac{(X_B - X_A)}{(Z_B - Z_A)} = \frac{(X_T + S\,x_2 - X_A)}{(Z_T + S\,z_2 - Z_A)},\quad \frac{(Y_B - Y_A)}{(Z_B - Z_A)} = \frac{(Y_T + S\,y_2 - Y_A)}{(Z_T + S\,z_2 - Z_A)} \quad (10)$$

Combining Equations 9 and 10 produces the two independent constraints as shown in Equations 11.

$$\frac{(X_T + S\,x_1 - X_A)}{(Z_T + S\,z_1 - Z_A)} = \frac{(X_T + S\,x_2 - X_A)}{(Z_T + S\,z_2 - Z_A)}$$
$$\frac{(Y_T + S\,y_1 - Y_A)}{(Z_T + S\,z_1 - Z_A)} = \frac{(Y_T + S\,y_2 - Y_A)}{(Z_T + S\,z_2 - Z_A)} \quad (11)$$

The two equations in Equations 11 can be written for each line in one dataset and its conjugate in the other. Consequently, two pairs of line segments yielding four equations are required to solve for the four unknowns. If the lines were intersecting, the shift components can be estimated (using the intersection points) but the scale factor cannot be recovered. As a result, at least two non-coplanar line segments are needed to recover these parameters. In summary, a minimum of two non-coplanar line segments is needed to recover the seven elements of the 3-D similarity transformation.

3. EXPERIMENTAL RESULTS

Two photogrammetric and one LIDAR datasets were involved in the study. Table 1 summarizes the properties of the photogrammetric datasets. The LIDAR dataset was captured using an OPTECH ALTM 3100 laser scanner with an average flying altitude of 975 m and average point density of 2.24 point/m^2. The first and last responses were recorded; and range and intensity data have been collected as well. According to the sensor and flight specifications, 0.5 m horizontal and 0.15 m vertical accuracies are expected. Range and intensity images are generated through interpolating the scattered points using two interpolation schemes coded as I1 (pixel size of 0.3 m and 4 m-radius search window using 2nd degree inverse distance weighting interpolation) and I2 (pixel size of 1.0 m using nearest neighbour interpolation.)

	1st aerial dataset	2nd aerial dataset
Camera used	RC-10 analogue	SONY F717 digital
Focal length (mm)	153.167	11.6761
# of images	6	17
Avg. flying height (m)	975	737
Avg. base (m)	540	221
Pixel size (mm)	0.024	0.004
Image measurement accuracy (mm)	± 0.024	± 0.004
Expected accuracy (assuming one pixel measurement error)		
planimetric (m)	0.15	0.25
vertical (m)	0.39	1.19
spatial (m)	0.42	1.22

Table 1: Specifications of the photogrammetric datasets.

3.1 LIDAR as control in photogrammetric triangulation

LIDAR - RC-10

Straight line segments extracted in LIDAR datasets I1 and I2 were used in separate experiments as the source of control information for the photogrammetric triangulation. Table 2 summarizes the quality of the aligned photogrammetric model through check point analysis. The results for the I2 dataset in Table 2 demonstrated some overall improvement either in the mean or standard deviation.

	LIDAR set I1	LIDAR set I2
# of control lines	80	79
# of check points	32	32
ΔX (m)	0.75 (±0.51)	0.65 (±0.28)
ΔY (m)	-0.10 (±0.43)	-0.15 (±0.26)
ΔZ (m)	-0.75 (±0.36)	-0.69 (±0.42)

Table 2: Check point analysis for LIDAR-RC-10 datasets.

LIDAR-SONY F717

Similar to the previous RC-10 experiments, straight line segments extracted in the two LIDAR datasets (I1 & I2) were used in separate experiments as the source of control information for the photogrammetric triangulation of the SONY F717 dataset. Table 3 summarizes the quality of the aligned photogrammetric model through check point analysis. Again, significant improvement is noticed in the y-coordinate while no improvement is seen in the other directions.

	LIDAR set I1	LIDAR set I2
# of control lines	72	72
# of check points	32	32
ΔX (m)	0.38 (±0.63)	0.42 (±0.70)
ΔY (m)	0.35 (±0.70)	0.20 (±0.67)
ΔZ (m)	-0.49 (±1.11)	-0.51 (±1.12)

Table 3: Check point analysis for LIDAR-SONY F717 datasets.

Comparing the results for the RC-10 dataset in Table 2 with that for SONY F717 in Table 3, it is clearly noticeable from the standard deviation values that RC-10 has a closer fit to the involved check points. This should be of no surprise since the expected accuracies based on the height-base ratio in Table 1 indicated such a trend. Inspecting Table 2 again for the improvement in results between I1 and I2 datasets, RC-10 shows better overall results when the LIDAR was interpolated with the 1.0 m pixel size using the nearest neighbour method (I2 set). This improvement can be attributed to the fact that the 1.0 m pixel size is closer to the 2.24 point/m^2 LIDAR point density (equivalent to 0.7 m pixel size), making it a more realistic sampling size. Table 3 shows that almost no change occurred between I1 and I2 interpolation sets for the SONY F717. Larger pixel size and lower level of detail in the SONY F717 images contributed to the steadiness in results as compared to the RC-10.

In another look at the results for RC10 in Table 2, the mean values of the differences clearly suggest the existence of biases especially in the *X*- and *Z*- directions. The fact that the mean values in the same table are well above the standard deviation values supports this finding. Table 3 also indicates some biases in the SONY F717 results, but the standard deviation of these values are larger than the mean values; hence no conclusion can be drawn about the existence of such biases in any of the directions.

3.2 LIDAR lines in the absolute orientation of the photogrammetric model

A separate photogrammetric model, using both point and straight line features, has been generated for RC-10 and SONY F717 imagery sets. The datum for each model was established using the coordinates of precisely surveyed ground control points. Hence the resulting photogrammetric models actually represent the real object space. LIDAR lines are then utilized as control information in an absolute orientation procedure to align the generated photogrammetric object space through a 3D similarity transformation. Assuming the LIDAR and ground control points used in the photogrammetric reconstruction both have the same reference frame, one can use the parameters of the transformation function directly to assess the quality of fit between the two datasets.

LIDAR - RC-10

Conjugate lines in photogrammetric and LIDAR datasets were identified and measured. There were eighty lines in I1, seventy nine in I2, and twenty three from manually identified and intersected planar patches. Table 4 lists the transformation function parameters between LIDAR and RC-10 models.

	I1		I2		Patch intersection	
Scale	0.999526	±0.00033	1.000097	±0.00025	1.000050	±0.00038
X_T (m)	0.62	±0.14	0.56	±0.11	0.53	±0.15
Y_T (m)	0.19	±0.15	0.04	±0.11	-0.11	±0.14
Z_T (m)	-0.98	±0.07	-1.07	±0.05	-0.86	±0.08
Ω (°)	-0.003	±0.014	-0.004	±0.010	0.029	±0.029
Φ (°)	0.030	±0.012	0.029	±0.009	0.083	±0.017
K (°)	-0.020	±0.018	0.009	±0.013	-0.023	±0.021

Table 4: 3D similarity parameters between LIDAR and RC-10 models.

The shift values in Table 4 for all sets indicate the existence of biases between the LIDAR and RC-10 datasets, thus confirming the results drawn from the first approach. After thorough investigation, it was found that RC-10 control points were recorded with respect to SAD 69 reference frame prior to 1998. On the other side, LIDAR data was based on SAD 69 after 1998 adjustments. Certain biases especially in the *X*- and *Z*-directions have been reported between the two versions. The overall normal vector between conjugate photogrammetric and LIDAR lines before and after absolute orientation is calculated and showed in Table 5. In this table, the best results were for linear features extracted using LIDAR planar patch intersection, followed by I2 and then I1 datasets.

	I1		I2		Patch intersection	
Before absolute orientation						
DX (m)	-0.26	±1.00	-0.24	±0.54	-0.23	±0.25
DY (m)	-0.15	±1.09	-0.01	±0.56	0.02	±0.20
DZ (m)	0.96	±0.64	1.01	±0.65	0.72	±0.37
After absolute orientation						
DX (m)	0.03	±0.96	0.04	±0.52	0.005	±0.13
DY (m)	-0.03	±1.04	0.02	±0.54	-0.057	±0.12
DZ (m)	-0.02	±0.45	-0.06	±0.46	-0.115	±0.41

Table 5: Overall normal vector between conjugate photogrammetric (RC-10) and LIDAR lines before and after absolute orientation.

LIDAR – SONY DSC-F717

Conjugate lines in photogrammetric and LIDAR datasets were identified and measured. There were sixty eight in each of I1 and I2 datasets. Table 6 lists the parameters of the 3D transformation function between the SONY and the LIDAR datasets.

	I1		I2	
Scale	0.999407	±0.0005	1.00015	±0.0006
X_T (m)	0.70	±0.19	0.69	±0.20
Y_T (m)	-0.09	±0.19	-0.08	±0.2
Z_T (m)	-0.63	±0.13	-0.69	±0.1
Ω (°)	-0.083	±0.037	-0.05	±0.027
Φ (°)	0.0005	±0.036	0.012	±0.026
K (°)	0.131	±0.039	0.076	±0.041

Table 6: 3D similarity parameters between LIDAR and SONY model.

Again, the consistent shift values in Table 6 suggest the existence of biases between the LIDAR and SONY F717 datasets. Also, the overall normal vector between conjugate photogrammetric and LIDAR lines before and after absolute orientation of this set is calculated and shown in Table 7, in which the standard deviations indicate LIDAR I2 dataset has the best result.

	Before absolute orientation				After absolute orientation			
	I1		I2		I1		I2	
DX (m)	-0.29	±1.08	-0.33	±0.69	0.08	±1.03	0.03	±0.60
DY (m)	-0.02	±1.08	0.05	±0.60	-0.07	±1.09	0.02	±0.59
DZ (m)	-0.52	±1.20	-0.57	±1.17	-0.11	±1.16	-0.12	±1.14

Table 7: Overall normal vector between conjugate photogrammetric (SONY F717) and LIDAR lines before and after absolute orientation.

4. CONCLUSIONS AND RECOMMENDATIONS

These experiments have demonstrated the compatibility of LIDAR and photogrammetric models generated by metric/analog and amateur/digital cameras. It also proved the usefulness of using LIDAR straight lines as a source of control for photogrammetric orientation. Straight-line features confirmed again its versatility in photogrammetric processes. An interesting conclusion is the feasibility of using LIDAR intensity images to collect necessary control for orienting photogrammetric models, although additional inaccuracies can be attributed to some difficulties and ambiguities when identifying linear features on the intensity image. The experiments also highlighted the role played by the sampling methodology through the choice of the interpolation method, grid size, and search space. The enormous extra computational effort and storage space spent to produce over-sampled grids inversely affected the reconstruction of the object space.

Further work is being undertaken to clarify a number of additional aspects arising from these experiments. This work includes the analysis and description of the discrepancy pattern between the true surface and generated LIDAR surfaces in the presence of various systematic errors. The two-step nature of the second approach can be utilised for this purpose. Also, experiments are being performed on the automatic extraction of the control features from the LIDAR data (intensity as well as range images). Another vital extension of the work is to investigate automatic correspondence among LIDAR and photogrammetric features. A logical application would be to develop methodologies for robust true ortho-photo generation that could handle relief displacements in large scale imagery over urban areas.

5. REFERENCES

Baltsavias, E., 1999. A comparison between photogrammetry and laser scanning, *ISPRS Journal of Photogrammetry & Remote Sensing*, 54(1):83–94.

Csathó, B. M., K. Boyer, and S. Filin, 1999. Segmentation of laser surfaces, *International Archives of Photogrammetry and Remote Sensing*, 32(3W14):73-80.

Ebner, H., and T. Ohlhof, 1994. Utilization of ground control points for image orientation without point identification in image space, *International Archives of Photogrammetry and Remote Sensing*, 30(3/1):206–211.

Filin, S., 2002. Surface clustering from airborne laser scanning data, *International Archives of Photogrammetry and Remote Sensing*, 32(3A):119-124.

Habib, A., Y. Lee, and M. Morgan, 2001. Surface matching and change detection using the modified Hough transform for robust parameter estimation, *Photogrammetric Record Journal*, 17(98): 303-315.

Habib, A., Y. Lee, and M. Morgan, 2002. Bundle adjustment with self-calibration using straight lines, *Photogrammetric Record Journal*, 17(100): 635-650.

Kilian, J., N. Haala, and M. Englich, 1996. Capture and evaluation of airborne laser scanner data, *International Archives of Photogrammetry and Remote Sensing*, 31(B3):383-388.

Lee, I., and T. Schenk, 2001. 3D perceptual organization of laser altimetry data, *International Archives of Photogrammetry and Remote Sensing*, 34(3W4):57-65.

Maas, H., and G. Vosselman, 1999. Two algorithms for extracting building model from raw laser altimetry data, *ISPRS Journal of Photogrammetry and Remote Sensing*, 54(2-3):153-163.

Postolov, Y., A. Krupnik, and K. McIntosh, 1999. Registration of airborne laser data to surfaces generated by photogrammetric means, *International Archives of Photogrammetry and Remote Sensing*, 32(3W14):95-99.

Schenk, T., 1999. Determining transformation parameters between surfaces without identical points, *Technical Report Photogrammetry No. 15*, Department of Civil and Environmental Engineering and Geodetic Science, OSU, 22 pages.

Schenk, T., and B. Csathó, 2002. Fusion of LIDAR data and aerial imagery for a more complete surface description, *International Archives of Photogrammetry and Remote Sensing*, 34(3A):310-317.

6. ACKNOWLEDGEMENTS

This research work has been conducted under the auspices of the GEOIDE Research Network through its financial support of the project (ACQ#HAB: SIACQ05).